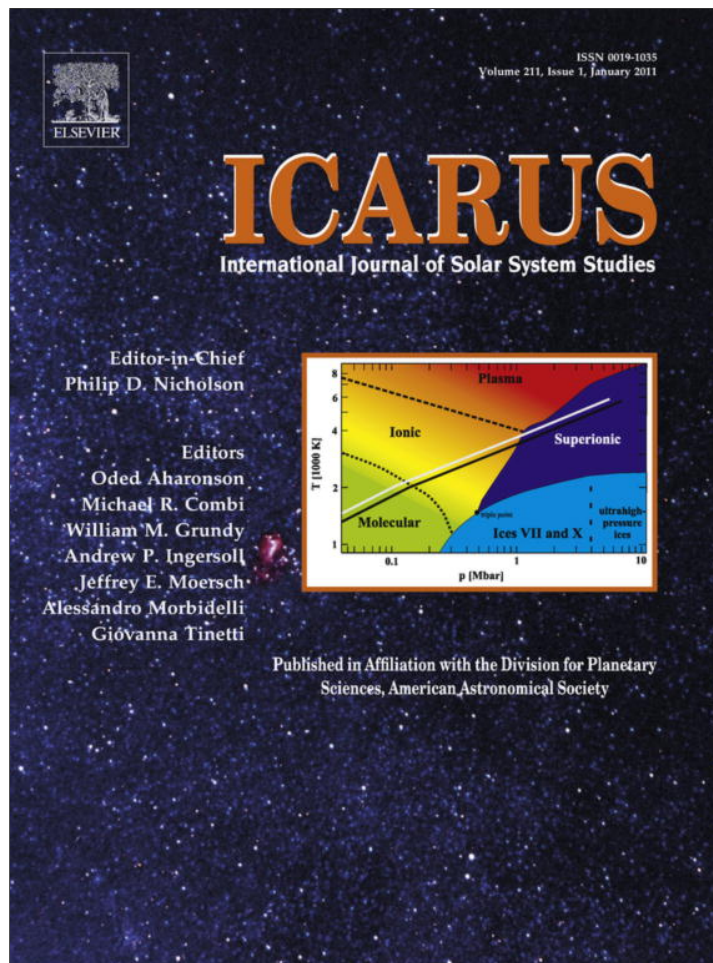


Provided for non-commercial research and education use.
Not for reproduction, distribution or commercial use.



This article appeared in a journal published by Elsevier. The attached copy is furnished to the author for internal non-commercial research and education use, including for instruction at the authors institution and sharing with colleagues.

Other uses, including reproduction and distribution, or selling or licensing copies, or posting to personal, institutional or third party websites are prohibited.

In most cases authors are permitted to post their version of the article (e.g. in Word or Tex form) to their personal website or institutional repository. Authors requiring further information regarding Elsevier's archiving and manuscript policies are encouraged to visit:

<http://www.elsevier.com/copyright>



Contents lists available at ScienceDirect

Icarus

journal homepage: www.elsevier.com/locate/icarus

Mineralogy and geochemistry of four lunar soils by laser-Raman study

Z.C. Ling^{a,b,c,*}, Alian Wang^b, Bradley L. Jolliff^b

^a School of Space Science and Physics, Shandong University, Weihai, Shandong 264209, PR China

^b Department of Earth & Planetary Sciences and the McDonnell Center for the Space Sciences, Washington University, St. Louis, MO 63130, United States

^c National Astronomical Observatories, Chinese Academy of Sciences, Beijing 100012, PR China

ARTICLE INFO

Article history:

Received 21 June 2010

Revised 24 August 2010

Accepted 24 August 2010

Available online 31 August 2010

Keywords:

Spectroscopy

Moon

Regoliths

Mineralogy

ABSTRACT

Laser Raman spectroscopy is used to investigate four lunar soils, focusing on mineralogy of grains of <45 μm size. Apollo samples 14163, 15271, 67511, and 71501 were selected as endmembers to study, based on their soil chemistry, maturity, and sample locations. Typical Raman spectral features for major and minor lunar minerals are discussed on the basis of major vibrational modes. We used the Raman peak shift to calculate Mg/(Mg + Fe + Ca) and Ca/(Mg + Fe + Ca) for pyroxene and Mg/(Mg + Fe) for olivine, and thus obtained the compositional distributions of these two minerals in each of the four lunar soils. Classification of feldspar grains was made based on recognition of their Raman patterns. A Raman point-counting procedure was applied to derive mineral modes of the soils, and these are found to be consistent with published modal analysis of these soils. The compositional distributions of pyroxene and olivine grains in each soil sample, as well as the mineral modes, reflect characteristics of the main source materials for these soils. Raman patterns and peak positions also reflect shock effects on plagioclase and quartz, found in 14163.

© 2010 Elsevier Inc. All rights reserved.

1. Introduction

1.1. Study of lunar soils

The lunar surface is blanketed by a mixture of unconsolidated rock, mineral and glass fragments, termed lunar regolith. Typically, the <1-mm grain-size fraction is referred to as “soil” (Heiken et al., 1991). Orbital remote sensing techniques mainly “see” this top layer of lunar regolith, and samples of it collected by Apollo and Luna missions provide “ground truth” for the remote sensing. Remote sensing, thus informed by the samples, can then be used to estimate the mineralogy and geochemistry of the lunar surface globally. Lunar regolith also contains the source materials for lunar resource utilization processes that will be used in future missions. As we enter a potential new era for lunar exploration, it is important to examine the Apollo and Luna samples by analytical techniques that could potentially be used in future lunar surface exploration and resource utilization.

There have been many mineralogical and geochemical studies of lunar regolith including rocks, mineral clasts, and glasses contained therein. Understanding the mineral and glass components and their characteristics (chemistry, shock effects, radiation alteration) are key to understanding remotely sensed spectra (Pieters

et al., 2000) as well as the diversity of source materials that have contributed to the regolith at a given location. The Lunar Soils Characterization Consortium (LSCC) (e.g., Taylor et al., 1996, 2001) applied point-counting techniques based on electron microprobe analysis to derive quantitative abundances of minerals in soil grain-size separates and coupled the results to reflectance spectra for the purpose of both validation of remotely sensed data and the development of spectral analysis tools. The optical properties of lunar soils differ from those of lunar rocks powdered in the laboratory (McCord and Adams, 1973; McCord and Johnson, 1970), thus it has been very important to understand the characteristics of the soils that lead to the spectroscopic differences. Such investigations have shown that it is the finest fraction of lunar soils (<45 μm) that dominates the optical properties of the bulk soil (Fischer and Pieters, 1995; Pieters et al., 2006, 1993).

Most previous petrographic studies of lunar soils are based on optical particle counts of the coarser fractions (Basu and McKay, 1979; Heiken and McKay, 1974; Simon et al., 1981). The size fractions that are most directly relevant for the remote sensing (<10 μm, 10–20 μm, 20–45 μm) are too small for traditional optical point-counting techniques. Thus Taylor et al. (1996) used X-ray mapping with an electron microprobe to determine the modal proportions of minerals and glasses in the <45 μm size range. Here, we use the laser Raman spectroscopy, which is a molecular vibrational spectroscopy, using a laser beam of ~1 μm diameter for Raman excitation. This method also has the capability to provide information on mineralogy, mineral proportions, and

* Corresponding author at: School of Space Science and Physics, Shandong University, Weihai, Shandong 264209, PR China. Fax: +1 607 255 6354.

E-mail address: zcling@sdu.edu.cn (Z.C. Ling).

compositional features of major lunar minerals for the fine portion of lunar soils (Haskin et al., 1997; Korotev et al., 1998; Wang et al., 1995). Some of the spectral characteristics reflect addition information such as identification of mineral polymorphs, shock effects, and crystallinity. Moreover, in comparison to other methods, which must be cast in appropriate experimental (sample preparation) context, laser Raman spectroscopy is most promising for mineralogical investigation of unprepared samples in the lab as well as for in situ planetary surface analysis.

1.2. Planetary Raman spectroscopy

Raman spectral patterns and major Raman peak positions are directly linked to the properties of chemical bonds in oxy-anionic groups of minerals (SiO_4 , CO_3 , SO_4 , PO_4 in silicates, carbonates, sulfates, phosphates, etc.) and their structural symmetry. Cation variations or substitutions in these minerals cause peak position shifts of major oxy-anionic groups. Compared to visible near infrared (Vis–NIR) spectra and thermal emission infrared (IR) spectra, the Raman spectral peaks of minerals are very sharp, non-overlapping, and less affected by the peaks from overtone and combinational modes. Therefore, straightforward mineral phase identification can be made, based on Raman spectral features in mixtures (soils and rocks) (Wang et al., 1995). The capability of laser Raman spectroscopy (LRS) for mineral identification and characterization of planetary materials has been demonstrated (Korotev et al., 1998; McMillan, 1984; Sharma et al., 2003; Wang et al., 1995). By using a Raman point-counting technique (Haskin et al., 1997), additional information on mineral proportions and rock textures can be obtained.

Calibrations have been done to extract compositional information from major igneous minerals using their Raman peak positions, e.g. Wang et al. (2001) for pyroxene, Kuebler et al. (2006) for olivine, Freeman et al. (2008) for feldspars, Jolliff et al. (2006) for phosphates, and Wang et al. (2004b) for Fe–Ti–Cr-oxides. These developments of planetary Raman spectroscopy make it a potential analytical technique for future planetary surface exploration of the

Moon, Mars, Venus, and asteroids (Sharma et al., 2003; Wang et al., 1995, 2003; Wdowiak et al., 1995).

In this study, we conducted a detailed LRS study, using a Raman point-counting procedure, on soil grains <45 μm in size of four lunar soils of different mineralogy and composition, i.e., Apollo 14163, 15271, 67511, and 71501. We present typical Raman spectra of all analyzed mineral species, derived chemical characteristics of the major minerals, and mineral modes for each soil sample.

2. Sample descriptions and experiments

The four lunar soils, 14163, 67511, 71501, and 15271 represent four extremes in lunar soil mineralogy and composition, with enrichments of KREEP-rich impact-melt materials (14163), feldspathic crustal materials (67511), high-Ti mare basalt (71501), and a low-Ti mare basalt with admixed KREEP-rich and feldspathic components (15271). The relation of these four soils is shown in Fig. 1.

Sample 14163 was collected from the Fra Mauro Formation by Apollo 14. It was collected at the end of EVA-1, northwest of the Lunar Module by scoop (Morris et al., 1983) and represents mixed material from the upper several centimeters of the regolith. The Fra Mauro formation is interpreted as impact ejecta from the Imbrium basin. This sample is strongly enriched in KREEP materials compared to the other Apollo soils (Laul and Papike, 1980; Taylor et al., 1972), although KREEP-rich, nonmare materials also occur in Apollo 12 soils. Sample 14163 contains abundant impact-melt breccias and includes several unusual lunar lithologies such as alkali anorthosite, granite, and monzogabbro (Jolliff, 1991; Jolliff et al., 1991). Sample 15273 was collected from station 6 on the Apennine Front (Morris et al., 1983). It consists of nearly subequal amounts of rock types representing the three apices of the mixing triangle shown in Fig. 1, i.e., a mixture of KREEP, mare, and feldspathic highlands materials. Apollo 16 sample 67511 was collected at station 11 on the rim of the very fresh North Ray Crater (Morris et al., 1983). The Apollo 16 mission was the only manned mission to obtain samples from a region of the ancient heavily-cratered

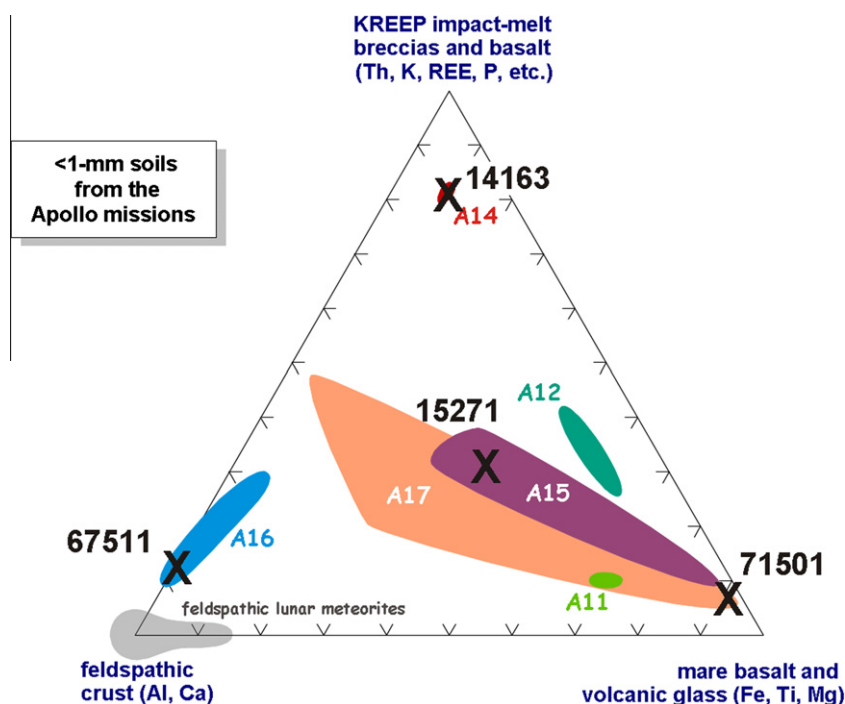


Fig. 1. Relationship of lunar soils composition to major groups of lunar rock types (Jolliff et al., 2000; Korotev et al., 2003).

highland crust (Muehlberger et al., 1980; Spudis, 1984; Jolliff and Haskin, 1995; Korotev, 1997). Apollo 17 sample 71501 was collected at station 1 on the Taurus–Littrow floor, 15 m northeast of a 10 m diameter crater with blocky ejecta. It has a dominant component as high-Ti mare basalt (Morris et al., 1983).

These four soil aliquots were subsampled from existing soil samples. Prior to Raman analysis, these subsamples were coarsely sieved with nylon meshes of $\sim 200 \mu\text{m}$ to remove coarse particles and to help prevent clumping. No other sample preparation was done except that the soil grains were lightly compacted in a shallow depression on a glass microscope slide specially designed for Raman analysis to provide a relatively flat surface.

Laser Raman spectroscopic measurements were made using a HoloLab 5000–532 nm laser Raman microprobe (Kaiser Optical System). The instrument has a spectral range of $50\text{--}4300 \text{ cm}^{-1}$, with a spectral resolution of $4\text{--}5 \text{ cm}^{-1}$. In this study, a $20\times$ microscopic objective with numerical aperture (NA) = 0.4 was used to condense a laser of $6 \mu\text{m}$ beam diameter onto the sample. An automatic scanning stage is attached to this Raman system to facilitate Raman point-counting (Haskin et al., 1997). In this procedure, Raman measurements were made on each sample over a $m \times n$ grid, with $\sim 100 \mu\text{m}$ intervals. About 100–200 spots were measured for each of the four soil samples. Although the samples were set up to have an approximately flat surface, manual adjustment of laser focus was made at each spot. The measurement of each spot typically took 12 s for acquisition and 10 accumulations, in order to obtain a spectrum with good signal-to-noise ratio. A laser power of 5 mW was used in general, but was reduced to 3 mW for opaque phases. The major Raman peak positions of olivine, pyroxene, and feldspar were obtained by spectral deconvolution with the aim of obtaining high accuracy in compositional calculations. GRAMS 32 software was used, with mixed Gaussian–Lorentzian peak shape, linear baseline, and the constraint-free iteration option

for fitting all parameters until convergence (or a minimum) was attained.

3. Grain-size distributions of four lunar soil samples

Photos of the four soils were taken with an Olympus SZH10 stereo camera (Fig. 2). Apollo soil 67511 is the brightest sample among the four, owing to its abundance of anorthositic material. Sample 71501 is the darkest of the four, owing primarily to abundant opaque ilmenite. Apollo soils 14163 and 15271 are intermediate in brightness.

Using the video camera attached to the microscopic stage of the HoloLab5000–532 nm Raman system, the diameter of each analyzed soil grain was estimated. Fig. 3 shows the grain-size distribution based on 100–200 measurements of each sample (generally in $10\text{--}40 \mu\text{m}$ size range). Soil 67511 (typically $\sim 30 \mu\text{m}$) is the coarsest, whereas soil 14163 is the finest (typically $10\text{--}20 \mu\text{m}$) among the four samples. These measurements agree with the distribution of grain sizes given in the Lunar Soils Grain Size Catalog (Graf, 1993). The differences in grain size reflect the maturity of these four soils, i.e., Apollo 14163 and 15271 are the most mature among the four soils (14163, $I_S/\text{FeO} = 57.0$; 15271, $I_S/\text{FeO} = 63.0$); 71501 is intermediate (“submature”, $I_S/\text{FeO} = 35.0$), and 67511 is the least mature soil ($I_S/\text{FeO} = 8.8$) (Graf, 1993; Morris, 1978).

4. Raman spectroscopic study of four lunar soil samples

4.1. Typical Raman spectra of lunar minerals

All lunar minerals have characteristic finger-print Raman spectra, thus mineral identification can be made at each sampling spot. Here we discuss the characteristic Raman spectra for lunar minerals in relation with their crystal structures and vibrational properties.

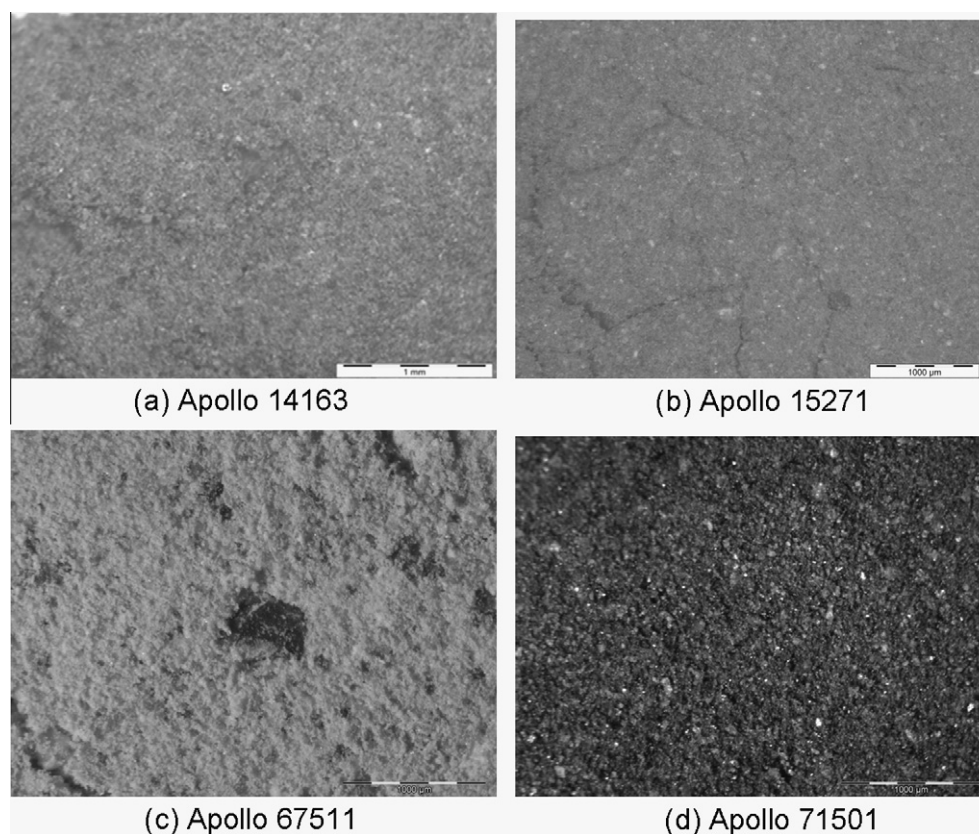


Fig. 2. Photos of lunar soils Apollo 14163, 15271, 67511 and 71501, respectively.

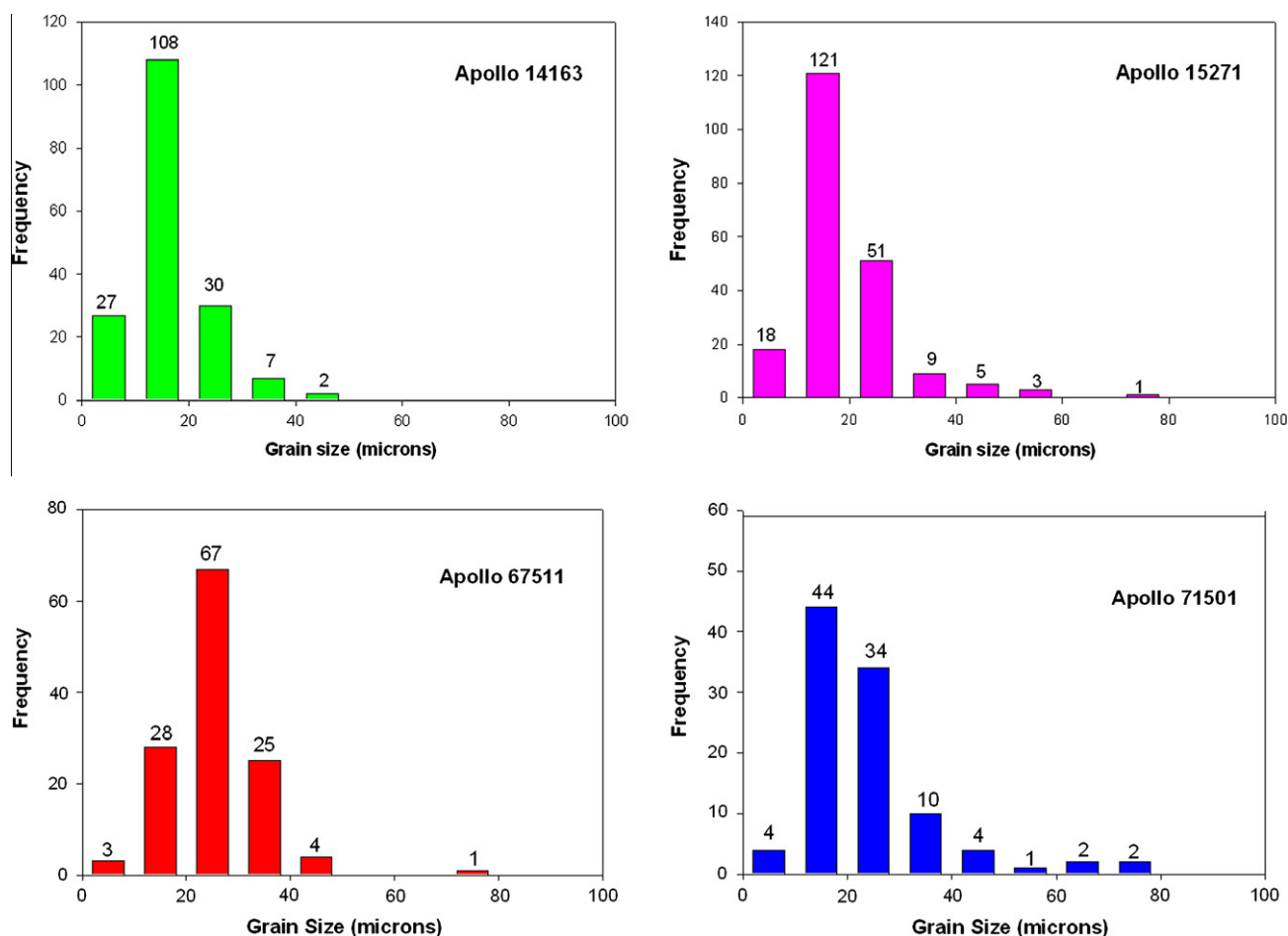


Fig. 3. Grain-size distribution of the four studied lunar soils as determined by the video camera on HoloLab5000-532 nm Raman system.

4.1.1. Raman features of pyroxene and extracting cation ratios in pyroxene

Pyroxenes are the most chemically complex silicates in lunar regolith and their chemistry records conditions of formation and evolutionary history of rocks from which they derive (Papike et al., 1998). Pyroxenes are compositionally variable solid solutions and lunar pyroxene are primarily “quadrilateral” [(Mg,Fe,Ca)₂-Si₂O₆] in compositions, defined within the compositional space bounded by enstatite, ferrosilite, diopside, and hedenbergite.

Raman spectra of lunar pyroxene have been obtained on Apollo samples (Fabel et al., 1972; Perry et al., 1972); they typically have two strong Raman peaks in the 1000–1010 cm⁻¹ and 650–670 cm⁻¹ spectral ranges. The ~1000 cm⁻¹ peak is assigned as the symmetric stretching vibration of the Si–O bond in [SiO₄] tetrahedra, and the ~670 cm⁻¹ peak is attributed to the symmetric stretching vibration of Si–O–Si bonds in [Si₂O₆]_n chains (White, 1975). Efforts to extract compositional information from pyroxene using Raman peak positions began in the early 1980s (e.g., Dele-Dubois et al., 1980; Ohashi and Sekita, 1982). Using a calibration established on the basis of co-registered Raman spectra and electron microprobe analyses (EMPA) on a set of pyroxene grains of lunar and martian origin, Wang et al. (2001) developed a method to calculate the Mg/(Mg + Fe + Ca) and Ca/(Mg + Fe + Ca) ratios of quadrilateral pyroxenes using these three Raman peak positions. Based on the above studies, we obtained geochemical properties of lunar pyroxene by using Raman point-counting method, in order to explore the potential of laser Raman Spectroscopy for in situ lunar researches.

As a chain silicate, pyroxene is easy to distinguish from other silicates (e.g., olivine and feldspar, as an orthosilicate and a frame-

work silicate, respectively), by a strong peak near 670 cm⁻¹ (Fig. 4). That peak for orthopyroxene is distinct as a doublet (near 670 cm⁻¹) from the singlet of clinopyroxene, reflecting two types of chain structures. The similar peak of clinopyroxene occurs at a longer wavelength, ~650 cm⁻¹. Generally, monoclinic pyroxenes (e.g., augite, diopside, hedenbergite, high T pigeonite) exhibit only one peak compared to double peaks of orthorhombic pyroxene (e.g., inverted pigeonite, enstatite, bronzite, hypersthene) (Wang et al., 2001).

In this study, we use the following Raman spectral features and three major Raman peaks to identify pyroxene (Opx and Cpx) in the four Apollo soils, and to calculate the cation ratios. They are as follows: a strong, asymmetric peak near 1000 cm⁻¹ as peak 1, a strong doublet or an asymmetric single peak near 670 cm⁻¹ as peak 2, and a group of strong, overlapping peaks around 320 cm⁻¹ as peak 3. As indicated by Wang et al. (2001), the two Raman component peaks in the ~1000 cm⁻¹ region have different symmetries, so the relative intensities of the two component peaks and the extent of their overlap can affect the apparent position of peak 1, thus caution is needed in the interpretation of these peak positions. In contrast, the positions of peaks 2 and 3 are less affected. The formula developed by Wang et al. (2001) was used in this study to calculate the cation ratios in pyroxene of the four samples:

$$v_i = a_i X^{\text{Mg}^{2+}} + b_i X^{\text{Ca}^{2+}} + c_i \quad (i = 2, 3)$$

where v_i is the position (in cm⁻¹) of Raman peak 2 or peak 3, $X^{\text{Mg}^{2+}} = [\text{moles Mg}^{2+}/(\text{moles Mg}^{2+} + \text{moles Fe}^{2+} + \text{moles Ca}^{2+})]$, $X^{\text{Ca}^{2+}} = [\text{moles Ca}^{2+}/(\text{moles Mg}^{2+} + \text{moles Fe}^{2+} + \text{moles Ca}^{2+})]$ (=Wo

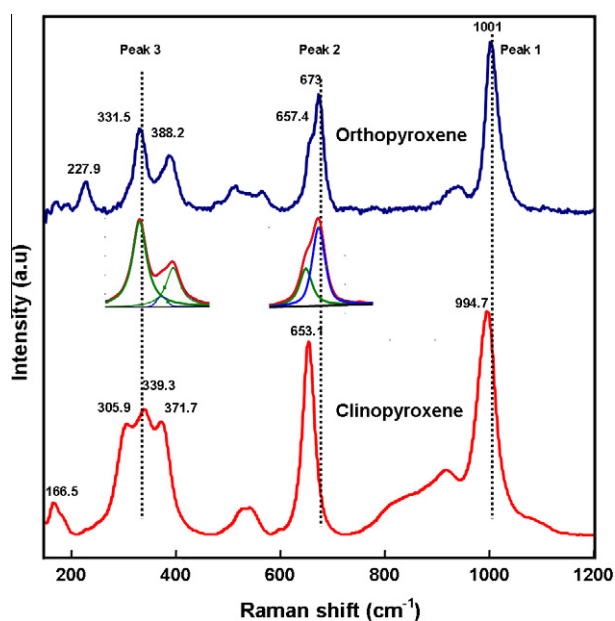


Fig. 4. Raman spectra of orthopyroxene and clinopyroxene, inset is an example for the peak fitting of peak 2 and peak 3.

content), and a_i , b_i , c_i are the coefficients determined by Wang et al. (2001).

4.1.2. Raman spectra of olivine and extracting Fo values

Olivine, $(\text{Mg,Fe})_2\text{SiO}_4$, has orthorhombic structure (Pbnm) and occurs in complete solid solution between the Fe and Mg endmembers (Papike, 1987). Because of its importance in terrestrial mantle research, olivine is well studied, both by infrared spectroscopy and by Raman spectroscopy (Chopelas, 1991; Iishi, 1978; Paques-Ledent and Tarte, 1973; Price et al., 1987). Fig. 5 shows a typical Raman spectrum of olivine, which can be reasonably divided into three spectral regions: $<400\text{ cm}^{-1}$, $400\text{--}700\text{ cm}^{-1}$, and $700\text{--}1100\text{ cm}^{-1}$. Peaks between 700 and 1100 cm^{-1} are attributed to the internal stretching vibrational modes of the SiO_4 ionic group, with the dominant feature as a doublet near 820 cm^{-1} and 850 cm^{-1} (Chopelas, 1991; Iishi, 1978). These features are frequently useful for identifying olivine in multi-phase spectra from igneous rocks and soils derived from igneous rocks (Wang et al., 1995, 2004a). Peaks in the $400\text{--}700\text{ cm}^{-1}$ spectral region result from internal bending vibrational modes of the SiO_4 ionic groups. Peaks below 400 cm^{-1} are assigned to lattice modes: rotational and translational motions of SiO_4 as a unit, and translational motions of octahedral cations (Mg^{2+} , Fe^{2+}) in the crystal lattice (Chopelas, 1991). The peaks in these two regions are normally much weaker than those in the $700\text{--}1100\text{ cm}^{-1}$ region, and are commonly not resolved in a spectrum from a multimineralic target.

For olivine, the molar or atom ratio of $\text{Mg}/(\text{Mg} + \text{Fe})$ (also called Fo value) is one of the most fundamentally important parameter to indicate its origin and crystallization process. Kuebler et al. (2006) presented a calibration to derive Fo value of olivine on the basis of co-registered Raman spectra and electronprobe micro-analysis (EPMA) on a set of olivine grains of terrestrial, lunar, and martian origin, using the peak positions of the doublet between 860 and 810 cm^{-1} . In this study, we apply the formula of Kuebler et al. (2006) to calculate the Fo of olivine grains in four samples.

$$\text{Fo}(\text{DB1}\&\text{DB2}) = y_3 + a_3x_1 + b_3x_2 + c_3x_1^2 + d_3x_2^2$$

where x_1 is the DB1 peak position, x_2 is the DB2 peak position, y_3 is the intercept, and a_3 , b_3 , c_3 , and d_3 are the coefficients listed in Table 4 of Kuebler et al. (2006).

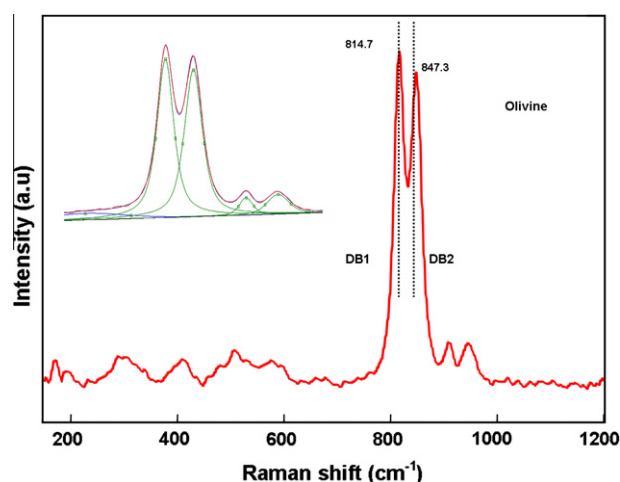


Fig. 5. Raman spectra of olivine, inset is an example for the peak fitting of the double peak.

4.1.3. Raman spectra of plagioclase and Or–Ab–An classification

Feldspar, mostly Ca-rich plagioclase, is the most common silicate mineral in the lunar crust. It has a framework structure made of three-dimensionally linked SiO_4 and AlO_4 tetrahedra (Papike, 1988). Among the tetrahedra, much larger sites with 8–12 coordination occur that accommodate larger cations such as Ca, Na, K, Fe, Mg, Ba. From K- (Or) and Na-endmembers (Ab) to Ca-endmember (An). The Si:Al ratio varies between 3:1 and 1:1. Ordering of Si and Al in specific tetrahedral sites can lead to complexities such as discontinuities in the feldspar structure. The formation temperature of feldspar affects its crystallinity and symmetry.

Numerous Raman studies have been done on naturally occurring and synthetic feldspars and glasses (Daniel et al., 1997; Matson et al., 1986; Mernagh, 1991; Sharma et al., 1983). In a comprehensive Raman, EMPA, and XRD study of 33 terrestrial feldspar samples, Freeman et al. (2008) developed a method to use LRS to discriminate seven major types of feldspar, including three endmembers orthoclase (Or), albite (Ab), and anorthite (An), as well as to distinguish the high and low temperature forms of some of them. Freeman et al. (2008) also determined that beyond these classifications, quantitative cation ratios (especially between Ab and An for lunar plagioclase) can not be extracted reliably from the Raman spectra of feldspar, because of the large size of octahedra or dodecahedra occupied by K, Na, and Ca.

Fig. 6 shows typical Raman spectra of feldspar obtained in the current study. Lunar plagioclase is generally depleted in Na relative to terrestrial plagioclase, as a reflection of the alkali-depleted composition of the Moon. We did, however, find a few grains of K-feldspar, and relatively sodic plagioclase (Na_{Ca} plagioclase) in the four Apollo soil samples.

We can separate the spectral characteristics of plagioclase into five groups as follows: Group I peaks appear in the spectral region of $450\text{--}520\text{ cm}^{-1}$, Group II peaks between 200 and 400 cm^{-1} , Group III peaks below 200 cm^{-1} , Group IV peaks between $600\text{--}800\text{ cm}^{-1}$, and Group V peaks between 900 and 1200 cm^{-1} . For the peak assignment, Group I shows the two prominent peaks in the $450\text{--}520\text{ cm}^{-1}$, which belong to the ring-breathing modes of the four-member tetrahedra. The Raman peaks in Groups II and III (below 400 cm^{-1}) belong to rotation–translation modes of the four-membered rings and cage-shear modes, respectively. The weaker peaks in the $900\text{--}1200\text{ cm}^{-1}$ region (Group V) were assigned to the vibrational stretching modes of the tetrahedra. Peaks from 700 to 900 cm^{-1} belong to the deformation modes of the tetrahedra (Freeman et al., 2008).

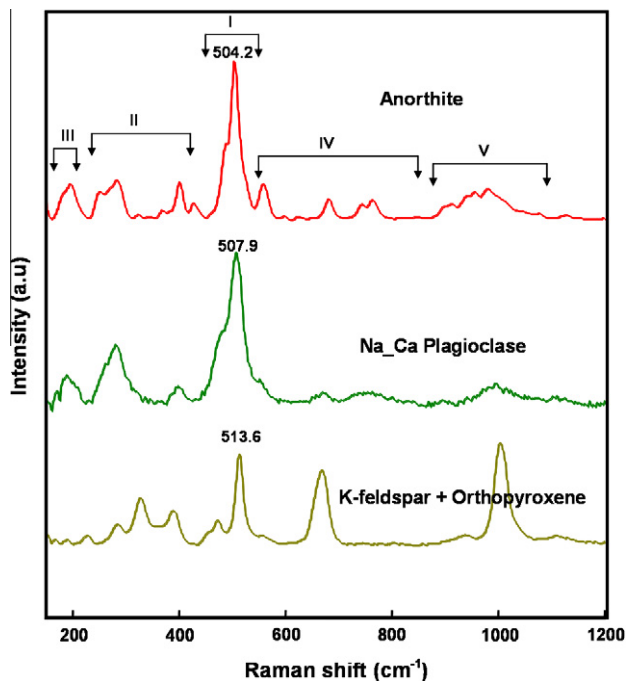


Fig. 6. Raman spectra of three typical plagioclase feldspar in lunar soils: Anorthite, Na_Ca Plagioclase and K-feldspar.

Plagioclase, and in particular, anorthite, is the main lunar feldspar. At room temperature, anorthite has a triclinic space group $P\bar{1}$ (Kempster et al., 1962; Megaw et al., 1962), commonly called low-temperature anorthite. As temperature increases, the crystal structure can be turned into a new phase (space group I) at 514 K due to a displacive transition (Daniel et al., 1995), leading to high-temperature anorthite. Angel (1988) found that such a transition can also occur at 2.6 GPa resulting from impact. Meteorite impact is of course an important surface process for soil evolution on the Moon, and the shock pressure produced by impacts can lead to a total or partial destruction of the crystalline structure of plagioclase, producing maskelynite or shocked anorthite (Johnson et al., 2002). These changes of the feldspar structure can all be characterized by Raman spectra, as shown in Fig. 7. Low-temperature anorthite has the most resolved and sharpest Raman peaks compared to the other two varieties considered here, which is an indication of its high degree of crystallinity. High-temperature anorthite has relatively fewer and broadened peaks, suggesting a reduction of cation ordering and crystallinity. The shocked anorthite shows broad and weak peaks (low S/N ratios), consistent with structural degradation and in some cases vitrification (formation of maskelynite) of this mineral.

4.1.4. Raman spectra of lunar ilmenite

With the ideal formula of FeTiO_3 , ilmenite is the most abundant oxide mineral in lunar regolith. The oxide minerals, although less abundant than silicates in lunar rocks, are significant because they retain signatures of conditions of formation (e.g., melt composition and f_{O_2}) of the rocks in which they occur. In addition, oxide minerals are obvious and important potential feedstocks for future production of oxygen and metals from lunar regolith during in situ resources utilization (ISRU) processes (Lewis and Lewis, 1987; Lewis et al., 1993; Mendell, 1985).

Ilmenite has a hexagonal structure that consists of alternating layers of TiO_6 and FeO_6 octahedra. Ilmenite produces relatively weak Raman signals compared to the silicate minerals, but was detectable during the Raman point-counting procedure used in

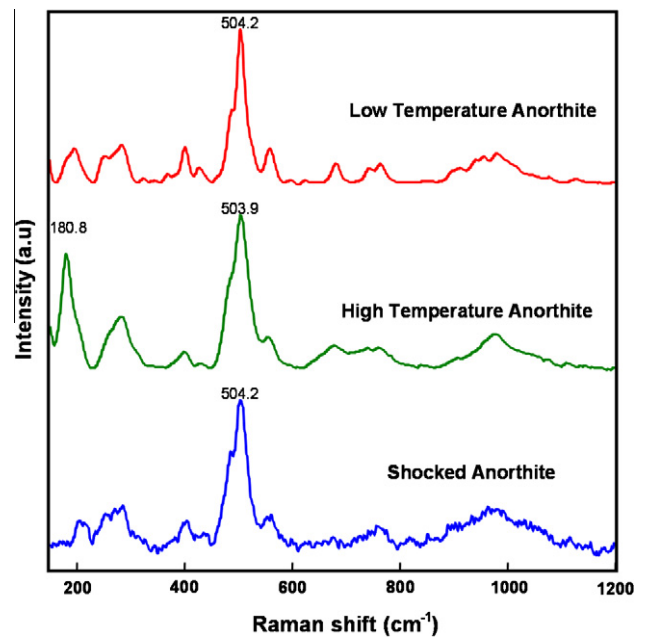


Fig. 7. The classification of anorthite mineral: Low-temperature anorthite, high-temperature anorthite and shocked anorthite.

this study. Numerous studies on the spectroscopic features of ilmenite have been reported (Chopelas, 1999; Linton et al., 1999; McMillan and Ross, 1987; Ross and McMillan, 1984). Wang et al. (2004b) reported a systematic Raman study of Fe-Ti-Cr-oxides, including an endmember ilmenite (FeTiO_3) and a partially Mg-substituted ilmenite (as is typical for lunar ilmenite).

Fig. 8 shows a Raman spectrum of ilmenite obtained in the current study. During preliminary Raman measurements, hematite was also identified; however, this could be an oxidation product of ilmenite when heated in air. When the laser power was decreased to about 3 mW on opaque phases, no hematite spectrum was obtained. Therefore, we ascribe the hematite spectra to ilmenite for the Raman point-counting analysis, which will be discussed in Section 4.3. Another potential source for the detection of hematite could be nanophase iron, Fe^0 , oxidized by the condensed excitation laser in air. Fe metal does not contribute to the Raman spectrum, although metal grains are ubiquitous in lunar soils (Noble et al., 2001).

4.1.5. Raman spectra of the SiO_2 polymorphs, quartz and cristobalite

Although rare on the Moon, the silica minerals are important indicators for the origin of some rocks and related geologic processes (e.g., red spots, domes) (Lucey et al., 2006). The commonly occurring silica polymorph in lunar basalt is cristobalite, which constitutes 5 vol.% of some basalt (Heiken et al., 1991). Quartz is only found in a few granite-like (felsite) clasts (Quick et al., 1981), or some coarse grained lunar granites occurring in rare fragments (Warren et al., 1983).

Quartz and cristobalite are silica polymorphs with different structures ($P3_121$ for quartz and $P4_12_12$ for cristobalite), thus they have completely different Raman spectral patterns (Fig. 9). The spectra can be divided into three regions, i.e., >1050 and $700\text{--}800\text{ cm}^{-1}$ (Si-O stretching modes), $350\text{--}500\text{ cm}^{-1}$ (O-Si-O bending modes), and $<300\text{ cm}^{-1}$ (Si-O-Si bending and torsional/twisting modes) (Etchepare et al., 1974). Cristobalite possess two predominant peaks at 410.8 and 228.6 cm^{-1} , whereas normal quartz peaks occur at 462.8 and 198.7 cm^{-1} , respectively.

Six Raman spectra of quartz (Fig. 9) were obtained from 14163 and 15271 soils. Typical low-temperature quartz has two sharp

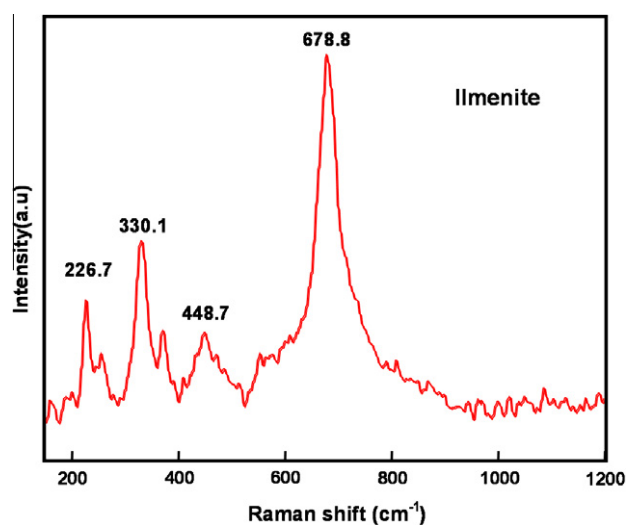


Fig. 8. Raman spectra of ilmenite in the four studied lunar soils.

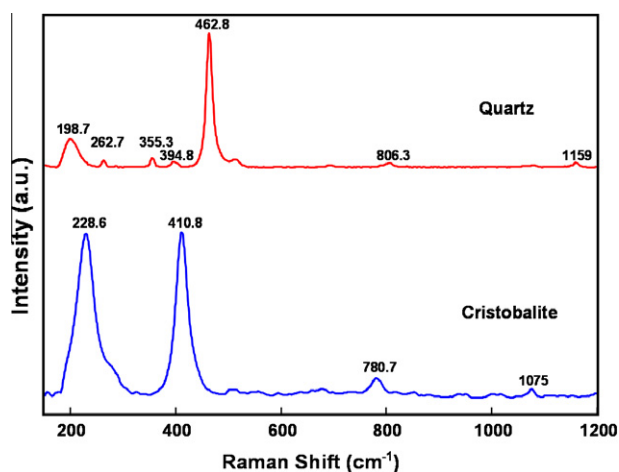


Fig. 9. Raman spectra of quartz and cristobalite in the four studied lunar soils.

and intense peaks at 464 and 206 cm^{-1} . Compared to low-temperature quartz, the major peaks (near 464 cm^{-1}) of all six lunar quartz spectra are shifted to lower peak positions with broadened peak widths. The change of Raman spectral features can be related to a distortion of the SiO_2 structural framework caused by shock metamorphism. There are many studies on pressure-induced Raman peak shifts for shocked quartz from terrestrial geologic settings and from laboratory experiments (see Fig. 10).

McMillan et al. (1992) carried out a Raman spectroscopic study of crystalline quartz samples shocked to peak pressures of 31.4 GPa, which shifted the major Raman peak from 464 cm^{-1} of unshocked quartz to 455 cm^{-1} . The largest Raman peak shift observed in our study of 14163 and 15723 soil samples is 457 cm^{-1} , suggesting the impact pressure experienced by these quartz grains should be less than 31.4 GPa.

4.1.6. Raman spectra of other lunar minerals

Phosphates are regarded as accessory minerals in most lunar rocks; however, they are major carriers of rare-Earth elements (REE). Fig. 11 shows a Raman spectrum of apatite [$\text{Ca}_5(\text{PO}_4)_3$] found in the lunar soil samples. In this study, we did not encounter REE-merrillite [$\text{Ca}_{16}(\text{Mg,Fe})_2(\text{REE})_2(\text{PO}_4)_{14}$], which commonly occurs together in lunar rocks with apatite. Those two minerals often exist

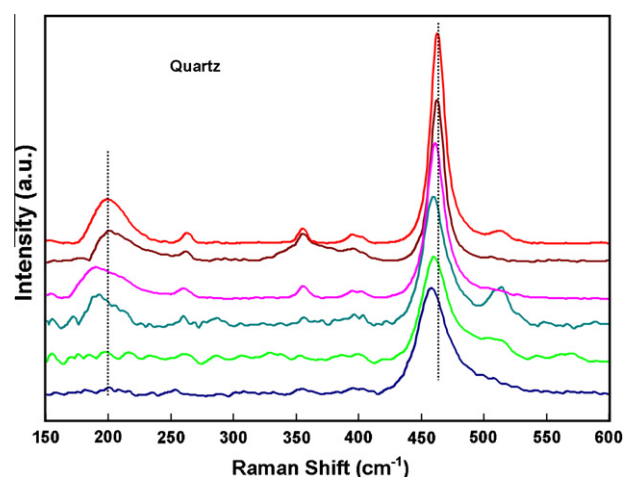


Fig. 10. Raman spectra of quartz obtained from Apollo 14163 and 15271. Note there are red shifts for the typical quartz peaks 464 and 206 cm^{-1} .

in late-stage mesostasis, commonly with K-rich glass, K-feldspar, ilmenite, zircon, fayalite, cristobalite, etc. (Papike et al., 1998). The phosphates are readily distinguished from other minerals by the sharp Raman peak at $\sim 960 \text{ cm}^{-1}$ (Jolliff et al., 2006), which corresponds to the stretching vibrational modes of PO_4 tetrahedra.

Glass, although technically not a mineral, is important geologically on the Moon, as a product of space weathering (micrometeorite impact) in agglutinates, as a shocked and molten product of the impact process, and as a product of pyroclastic eruptions. The lower spectrum in Fig. 11 shows a glass peak centered at 859 cm^{-1} , which can be assigned as a Si–O stretching mode in the short-range-ordered structure.

4.2. Compositional characters of major silicate minerals

Based on the methods described in Section 4.1, $\text{Mg}/(\text{Mg} + \text{Fe} + \text{Ca})$ and $\text{Ca}/(\text{Mg} + \text{Fe} + \text{Ca})$ ratios of each pyroxene grain and $\text{Mg}/(\text{Mg} + \text{Fe})$ ratio of each olivine grain encountered during Raman point-counting were calculated from their Raman peak positions. Furthermore, weighted compositional distributions of pyroxene (and olivine) in each of the four lunar soil samples were obtained and are presented in the following section. The classification of feldspar in each sample was also made according to the method described above.

4.2.1. Pyroxene and olivine – cation ratios and weighted compositional distributions

The $\text{Mg}/(\text{Mg} + \text{Ca} + \text{Fe})$ and $\text{Ca}/(\text{Mg} + \text{Ca} + \text{Fe})$ ratios of each pyroxene grain and $\text{Mg}/(\text{Mg} + \text{Fe})$ ratio of each olivine grain encountered during the Raman point-counting were calculated using the formulae discussed in Section 4.1. Accurate Raman peak positions obtained through spectral curve fitting were used for these calculations. Values of $\text{Mg}/(\text{Mg} + \text{Fe} + \text{Ca})$ of pyroxene in the Mg–Fe–Ca quadrilateral can be determined with an accuracy of ± 0.1 . The precision for $\text{Ca}/(\text{Mg} + \text{Fe} + \text{Ca})$ values derived from the Raman data is about the same except that corrections must be made for very low-Ca and very high-Ca samples (Wang et al., 2001). For olivine, the two-peak calibration is capable of determining olivine compositions to within ± 10 Fo units (Kuebler et al., 2006). These calculations enable us to plot each pyroxene grain into En–Di–Hd–Fs quadrilaterals for the four soil samples (Fig. 12). The data points in these drawings are classified into two types, with “good points” obtained from the single-phase spectra (pyroxene in this case) or from multi-phase spectra without obvious overlap with a feldspar peak at 320 cm^{-1} .

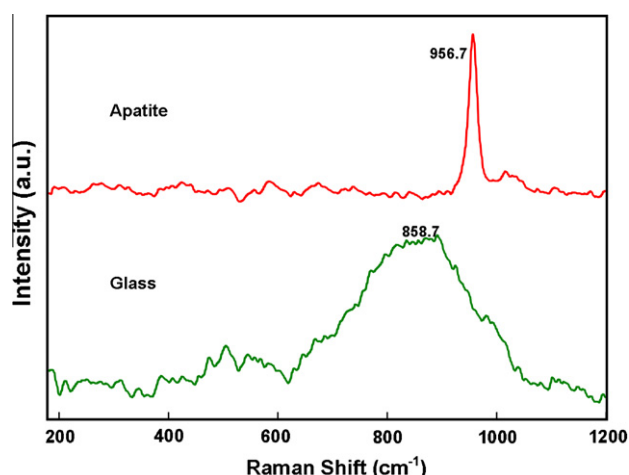


Fig. 11. Raman spectra of apatite and glass in the four studied lunar soils.

The pyroxene grains in sample 67511 (fresh anorthositic high-land soil) are slightly richer in Mg than other soils, which is consistent with Raman-derived mineral modes (Opx > Cpx, Section 4.3.1). In 71501 (high-Ti mare soil), pyroxene grains are slightly

richer in Fe and there are more augite grains than pigeonite. The pyroxene grains in sample 14163 have a wider Mg–Fe compositional range than 67511, whereas in 15271, the pyroxenes show a wide separation in Ca contents that is almost bimodal.

Owing to the relatively smaller number of olivine grains encountered during the Raman point-count procedure of each sample, the compositional trends are less evident. For 67511, the olivine composition is distributed between Fo₂₀ and Fo₆₀. There are very few data for olivine in KREEP-rich soil 14163; however, most good points are near Fo₃₀. We can tentatively say that 15271 has a wide range of olivine compositions from Fo₀ to Fo₈₀, which reflects the mixed nature (mare + highlands) of this soil.

By combining the information from Raman peak positions and the frequency of encountering pyroxene (or olivine) during the Raman point-count procedure, we obtain a weighted compositional distribution of pyroxene (or olivine) in a particular lunar soil sample. That distribution demonstrates the compositional character of the majority of pyroxene grains and may also serve to indicate the source or sources of pyroxene grains in the sample. Fig. 13 shows the weighted compositional distribution of pyroxene grains for the four samples of this study in terms of the Mg/(Mg + Fe) ratio (as Mg# in the following discussion) calculated on the basis of their Raman peak positions. The figure demonstrates that the majority of pyroxene grains (82%) in 67511 have Mg# > 0.5. Conversely,

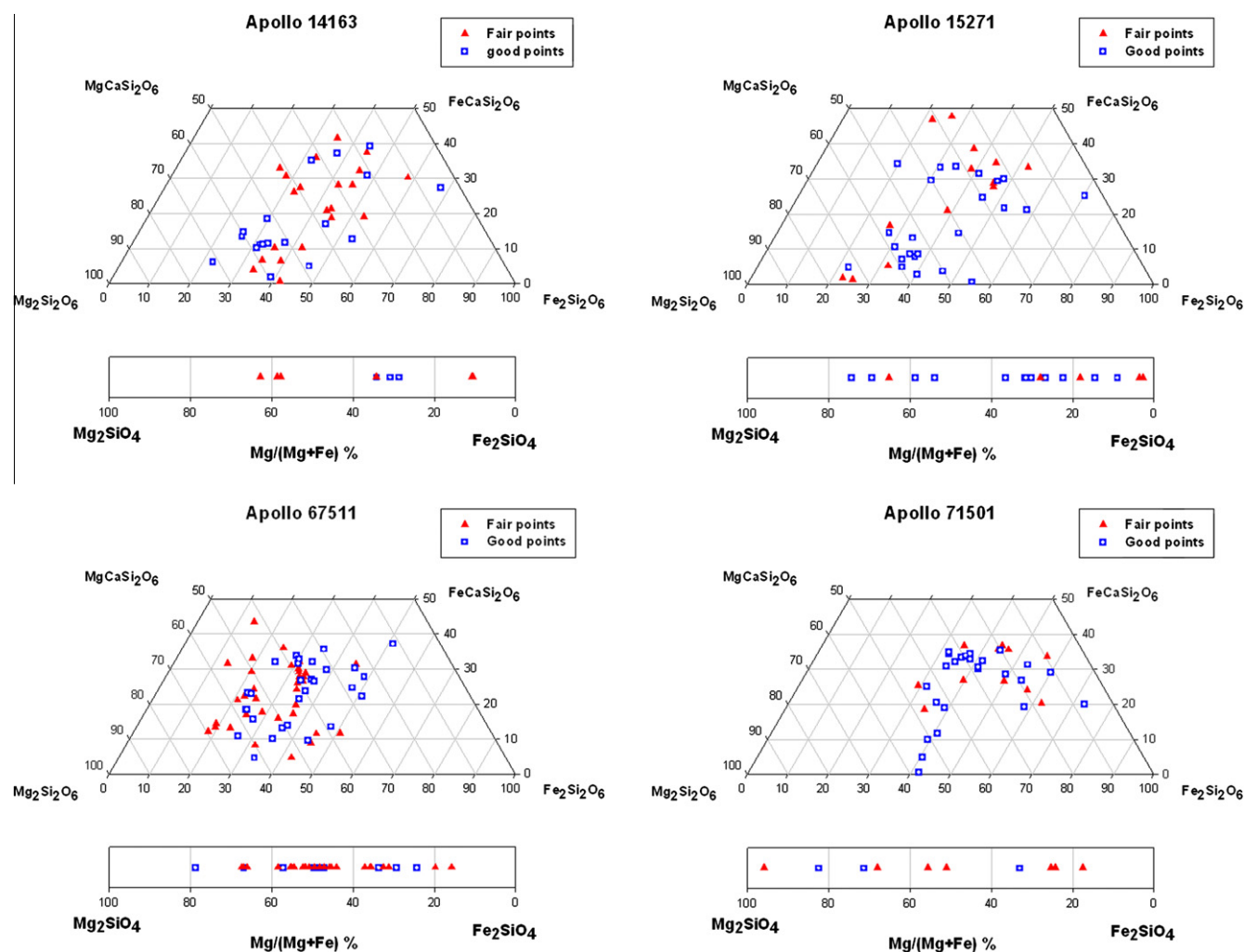


Fig. 12. The pyroxene quadrilaterals of the four lunar soils, the points are divided into good and fair points by estimation of the peak fitting results. The good points are from the spectra without obvious overlap with feldspar in 320 cm⁻¹ spectral range thus refer to have better peak fitting during the calibration procedures, thus more reliable results are expected than those of fair points.

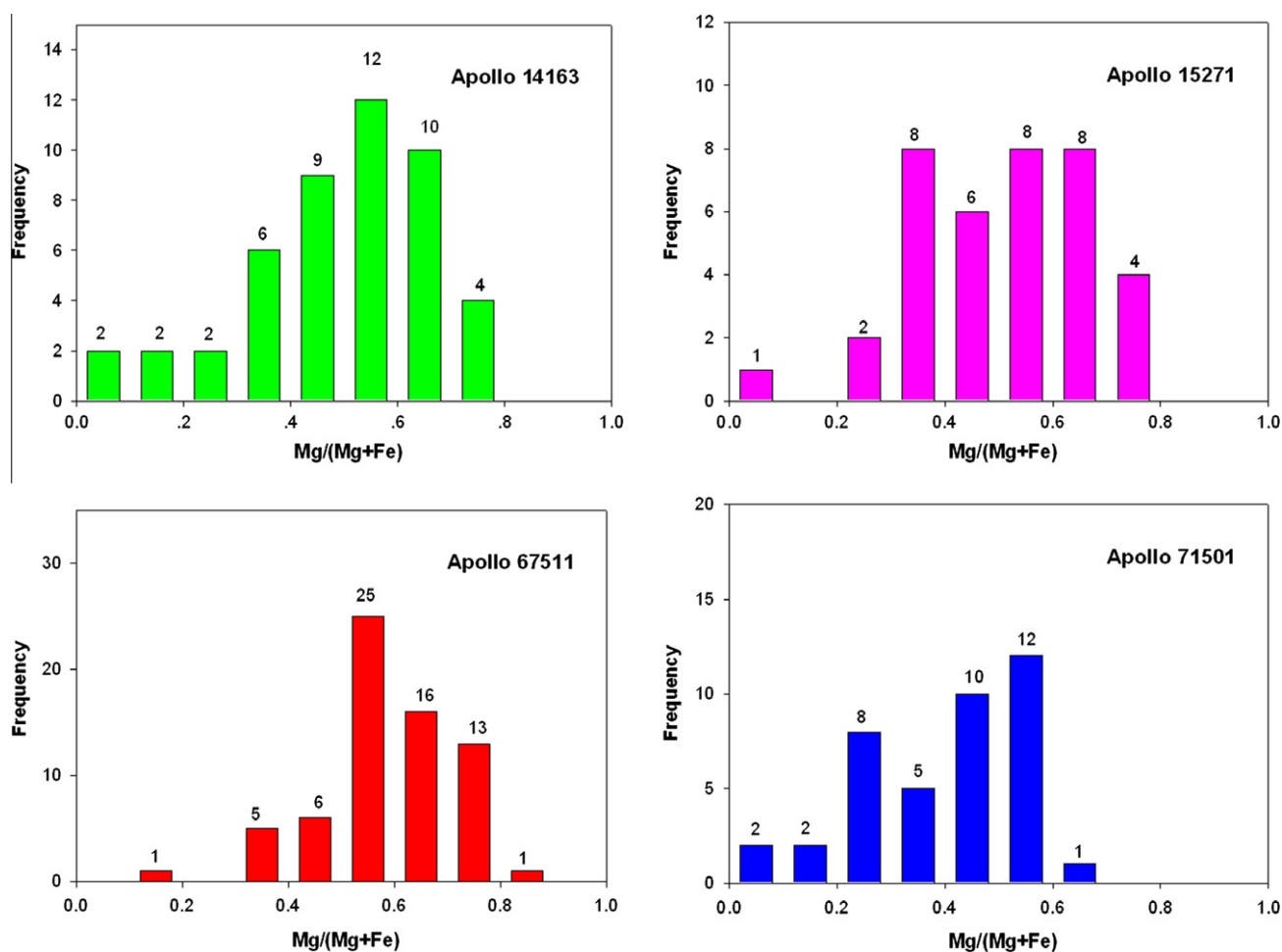


Fig. 13. Histogram of Mg/(Mg + Fe) for pyroxene among the four soils.

pyroxene grains in 71501 are Fe-rich: 68% have Mg# <0.5, as expected for a mare basalt. In addition, the histogram for 71501 shows a nearly bimodal distribution, with one peak near Mg# ~0.2 and another peak near Mg# ~0.5. This bimodal behavior matches with the data distribution in the Mg–Fe–Ca quadrilateral (Fig. 12), where the data points in the Fe-rich part have intermediate Ca contents, in contrast with the data in the middle-Fe part, which have low- to medium-Ca values. In 14163, 87% of the pyroxene grains have Mg# of 0.3–0.8 and show a normal distribution centered at Mg# 0.55, with a few outliers at the Fe-rich end. The normal distribution indicates a single type of pyroxene formation process in the source region(s) of this soil. It is interesting to compare this shape with the shape of the weighted compositional distribution of pyroxene in 15271, which shows a broad, non-peaked distribution in the same Mg# range (0.3–0.8). The 15271 distribution in Mg/(Mg + Fe) is consistent with the mixed nature of this soil, i.e., from multiple sources with very different compositional characteristics (mare and highlands sources).

4.2.2. Feldspar—classification of feldspar in each sample

Based on the criteria built on Raman spectral features described in Freeman et al. (2008), the feldspar grains encountered during our Raman point-counting were classified into five groups, as shown in Fig. 14. For this classification, the discrimination of K-feldspar, Na–Ca plagioclase, and anorthite is based on peak positions, whereas further classification of the anorthite group requires evaluation of the peak shapes. In 14163 and 15271, plagioclase is more sodic than in the other two samples. Shocked anorthite is

rare in 67511, consistent with the low maturity of this soil. In addition, among all types of feldspar found in this sample, >90% are low-temperature anorthite, compared to 13.2%, 26.5%, and 14.7% in other three samples. Among the four soil samples, 71501 has the greatest percentage of high-temperature anorthite (38%), which is 2–20 times higher than the percentages of high-T anorthite in the other soils (Fig. 14). This characteristic is consistent with a primarily volcanic origin for most of the plagioclase in 71501. High-temperature anorthite grains in 14163 and 67511 are uncommon. As for the KREEP-rich soil 14163, it is on average more sodic and has the most K-feldspar of the four soils. This observation agrees well with the fact that Apollo 14 samples include igneous lithologies with evolved compositions such as granite and quartz monzogabbro (monzodiorite) (Jolliff, 1991). Shocked anorthite constitutes a large portion of the mineral grains in 14163, 15271, and 71501 (nearly 40%), reflecting the more mature nature of these three soils compared to 67511. In 15271, the compositions of olivine and pyroxene, and the feldspar characteristics (percentages of low-T and high-T anorthite, and Na–Ca-plag) are between the extremes of the other three soils, consistent with the mixed nature of this soil (i.e., a mixture of the basaltic, KREEPy, and highly feldspathic soils).

4.3. Mineral modes for the four typical soils

After mineral identifications based on above discussions, we performed a modal analysis using the Raman point-counting method. The number of occurrences is given for each mineral

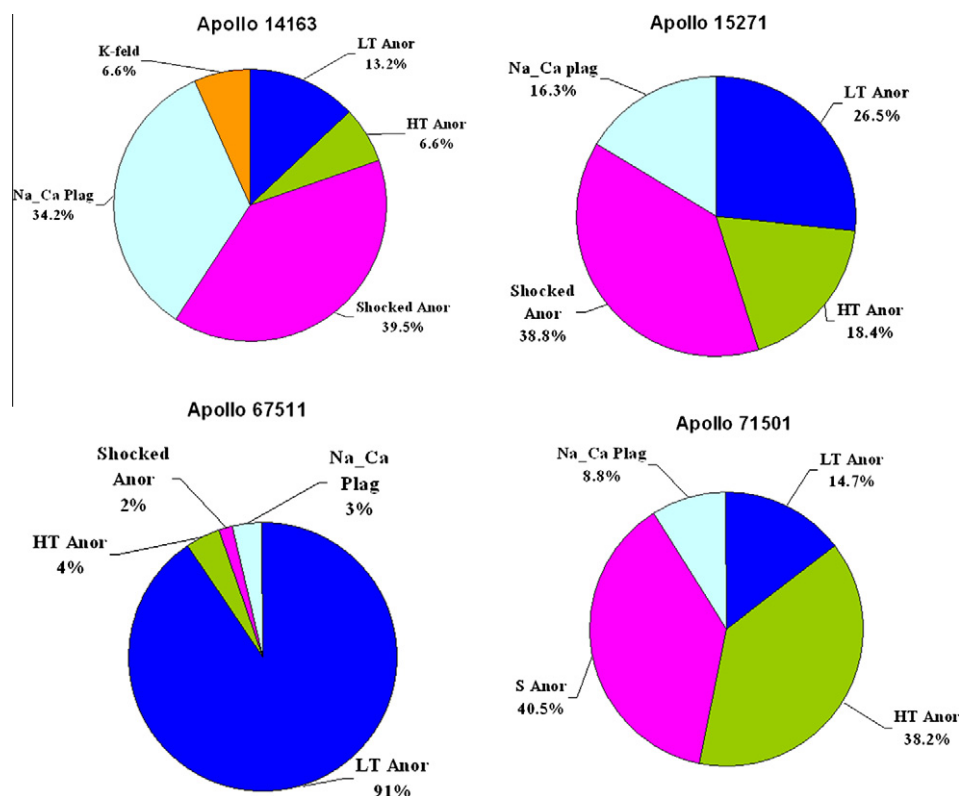


Fig. 14. The distribution (vol.%) of feldspar in four lunar soils as determined by Raman point-counting method.

according to respective point Raman spectra. For a few points in which two or three minerals were present (in a given spectrum), 1/2 or 1/3 occurrence was assigned to each mineral. The mineral modes of four lunar soils were shown in Fig 15.

4.3.1. Mineral modes of the four soil samples based on Raman point-counting

Mineral mode results based on Raman point-counting analysis (Fig. 15) indicate that plagioclase is the most abundant mineral in all four of the soil samples, with 67511 having the highest content (56.6 vol.%) and 71501 the lowest (25.6 vol.%). These results are in general agreement with the understanding that the typical feldspathic highlands (e.g. 67511) are mainly composed of plagioclase feldspar. However, highland sample 67511 (an immature soil excavated by the impact of North Ray Crater) seems to contain more mafic minerals (56.6% plagioclase) than the typical highland rocks (ferroan anorthosites, >90% plagioclase). Because 67511 has a large grain-size range (centered at 30 μm , Fig. 2) and is immature, it may represent the composition of highland soils not so contaminated by meteorite impacts. In addition, the soils collected from North Ray crater are not typical mature highland soils, because the time elapsed since the crater was formed (50 myr) is not enough for the crater ejecta to become mature (Morris, 1978). Sample 14163 contains 33.4% plagioclase. The percentage of plagioclase (25.6%) in soil 71501 is less than the total percentage of pyroxene (33.3%), which is consistent with the mare basalt origin of 71501 (Heiken et al., 1991). Orthopyroxene is richer than clinopyroxene in highland soil 67511 and clinopyroxene is richer than orthopyroxene in 71501, whereas orthopyroxene and clinopyroxene are almost equal in 15271 and 14163. These distributions follow the general pattern of highlands and mare rocks in that highland soil 67511 contains more orthopyroxene and mare soil 71501 has more clinopyroxene. Olivine is less abundant (4.7%) in KREEP-rich 14163, whereas highland soil 67511 contains the highest percentage of olivine (10.4%) among the four soils.

Soils 14163 and 71501 have greater amounts of glassy materials than soil 67511. Raman point-counting indicates that the glass is 3.8% in 67511 but that it is nearly 20% in 14163 and 15271. This distribution reflects the maturity of each soil, i.e., the maturity increases in the following order: 67511 ($I_S/FeO = 8.8$) < 71501 ($I_S/FeO = 35$) < 14163 ($I_S/FeO = 57$), 15271 ($I_S/FeO = 63$) (Morris, 1978).

We found six spectra of quartz in 14163 and 15271 soils. Our Raman point-count studies of 14163 and 15271 suggest that quartz accounts for 1.4% of the overall mineral modes, and cristobalite, 0.5% for soil 15271.

From the mineral modes of the four soils, 67511 has the highest plagioclase proportion; soil 71501 is a typical high-Ti lunar mare soil as indicated by the lowest plagioclase and highest proportions of ilmenite; 14163 is a low-Ti KREEP endmember as indicated by the very low proportions of ilmenite and high proportions of KREEP component such as K-feldspar and phosphate. The mineral mode of 15271 reflects the mixed nature of this soil.

4.3.2. Comparing the mineral modes of 14163 and 71501 soils obtained by Raman point-counting to those obtained by X-ray imaging

Earlier modal analyses of lunar soil were usually done by "particle counting" with optical petrography or electron microprobe methods (e.g., Simon et al., 1981; Heiken and McKay, 1974). These analyses provide a classification of soil fragments (e.g., pyroxene, basalts, breccias, agglutinates), but they do not provide information on mineral modes in multi-phase lithic fragments and fused-soil particles (e.g., agglutinates) (Lucey et al., 2006). To validate the mineral mode of lunar soils by Raman point-counting, we first compare the mineral mode of soil 14163 with the results of earlier optical and microprobe measurements (Simon et al., 1981; Carr and Meyer, 1972; Finkelman, 1973; Labotka et al., 1980) (Table 1). Considering different ranges of grain size and analytical methods, the resulting discrepancies of these measurements is to be expected. However, relatively good matches of major

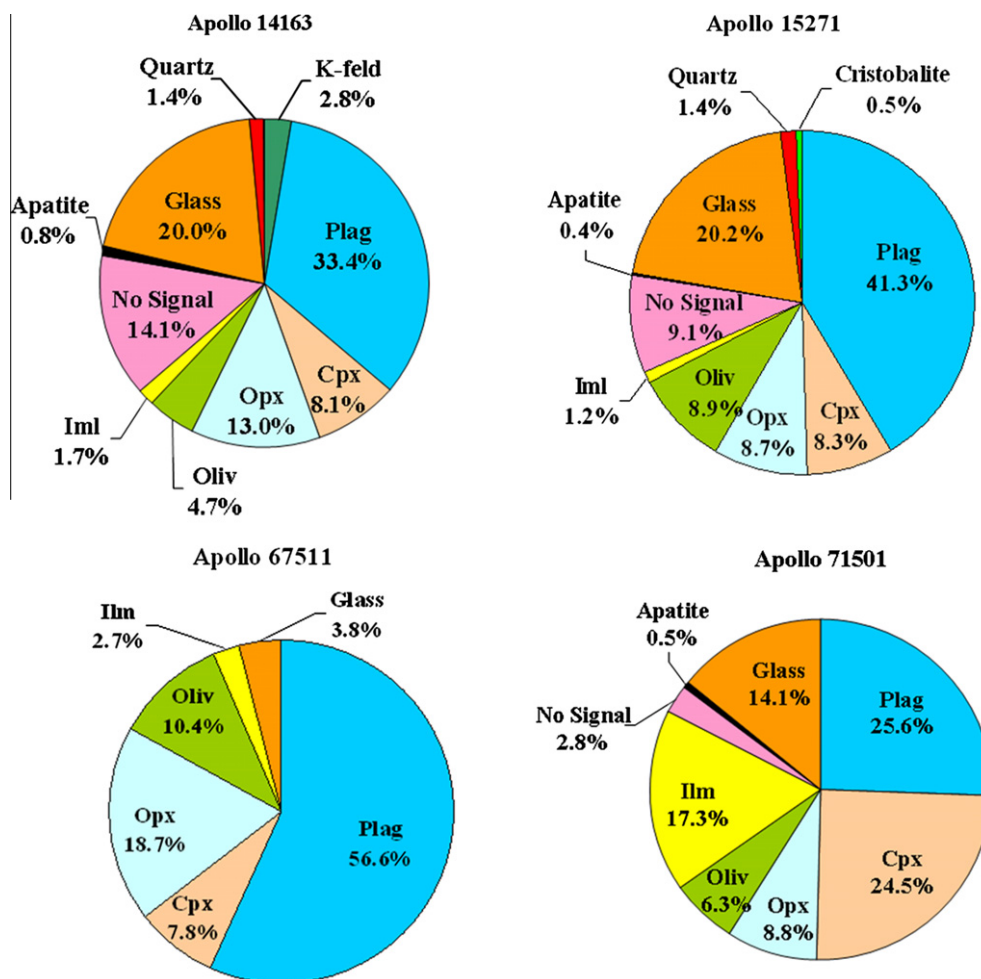


Fig. 15. Mineral modes (vol.%) of the four lunar soils as determined by Raman point-counting method.

minerals can be found between our results by Raman point-counting and those by Finkelman (1973) and Labotka et al. (1980), who used microprobe methods for analysis of relatively fine soils (<90 μm),

As a second step, we compare our results in detail with the more accurate results done by the LSCC with X-ray imaging methods (Taylor et al., 2001; Pieters et al., 2006), taking 14163 and 71501 as examples (Table 2). It is important to note that the mineral modes and mineral chemistry of the same lunar soil differ in different grain-size ranges, thus comparison is better done for similar grain-size ranges. For 14163, a weighted average mineral mode was taken over the three sets of LSCC results corresponding to

three grain-size distributions of <10 μm, 10–20 μm and 20–45 μm, using 15.5%, 62.1% and 22.4% as weights respectively. For 71501, an equal weighted average mineral mode was taken over two sets of X-ray results corresponding to two grain-size distributions of 10–20 μm and 20–45 μm. These two mineral modes are compared with our results obtained by Raman point-counting on 14163 and 71501 soils, respectively.

Compared to the results from the LSCC work, we overestimate the abundance of pyroxene and olivine, and underestimate the plagioclase. Raman spectroscopy provides information on the minerals excited by the laser beam to yield Raman peaks. The Raman

Table 1

Comparisons of mineral modes (vol.%) for lunar soil 14163 between earlier optical and microprobe studies with Raman point-counting method.

References	Simon et al. (1981)	Carr and Meyer (1972)	Finkelman (1973)	Labotka et al. (1980)		This work
Size	1000–90 μm	1000–70 μm	<37 μm	90–20 μm	20–10 μm	<45 μm
Method	Optical ^a	Optical	Microprobe	Microprobe		Raman
Plagioclase	5.1	5.1	18.0	17.2	18.3	33.4
Pyroxene	2.6 ^b	4.1	31.0	10.2	29.3	21.1
Olivine		0.4	4.5	3.5	5.2	4.7
Ilmenite			2.5	0.5	2.0	1.7
Glass	10.3	61.1	36.0	22.4	26.1	20.0
Others	81.9	29.2	8.0	46.2	19.1	19.1
Total	99.9	99.9	100	100	100	100
PX/Plag	0.51	0.80	1.72	0.59	1.60	0.63

^a For optical method, we concentrate on the mineral fragments and let out of the other lithic fragments.

^b Denote the mafic phase in Simon et al. (1981).

Table 2
The comparison of mineral modes (vol.%) for soil 14163 and 71501 got from X-ray imaging (XRI) by LSCC and Raman point-counting (RPC) method. Note that, modal mineral percentage of bulk soil from LSCC were recalculated based on the grain-size distribution of our results. The normative percentages were calculated by ruling out the glass components (Pieters et al., 2006).

Minerals	14163_XRI	14163_RPC	71501_XRI	71501_RPC	14163_XRI_Norm	14163_RPC_Norm	71501_XRI_Norm	71501_RPC_Norm
Plagioclase	19	33.4	18.1	25.6	46.6	41.8	35.4	29.8
Pyroxene	12.8	21.1	17.5	33.3	31.4	26.4	34.2	38.8
Olivine	1.9	4.7	3.5	6.3	4.7	5.9	6.8	7.3
Ilmenite	0.9	1.7	11	17.3	2.2	2.1	21.5	20.1
Glass	59.2	20	48.8	14.1				
Others	6.2	19.1	1.2	3.3	15.2	23.9	2.3	3.8
Total	100	100	100.1	99.9	100.1	100.1	100.2	99.8

signal strength is a function of the Raman-cross-section of a mineral phase, which depends on the covalency of the chemical bonding that produces the major Raman peaks. For example, the pyroxene and olivine have higher strength in Raman signals than opaque oxide mineral phases. It also appears that we overestimate crystalline minerals and underestimate the glassy component in lunar soils. There might be two potential causes: (1) Glasses have weaker Raman signals than crystalline minerals. (2) Those “glass” components of LSCC may contain crystal grains that can be detected by Raman but not XRI. To handle the discrepancy in glasses, we normalized the results by subtracting out the glass components and normalizing the crystalline components as shown in Table 2. The results of Raman point-counting agree well with XRI.

The Raman signal comes from a volume around and beneath the laser focal surface, i.e., depending on the transparency of a mineral grain for 532 nm radiation (olivine, pyroxene, feldspar, but not ilmenite). In some instances, mineral grains such as pyroxene and olivine beneath the grain at the surface (even under 30 μm thickness) can be detected and assigned as co-existing phases with the surface mineral (e.g., plagioclase). Furthermore, considering that many Raman inactive plagioclase phases (e.g., shocked anorthite) exist in lunar soils, we might underestimate the plagioclase and overestimate pyroxene and olivine. This could be the reason for our underestimate for plagioclase even after normalization (as shown for soil 71501), whereas for ilmenite, the difference is smaller. Finally, we only take around 100–200 spectra for each soil, which is fewer than done for X-ray imaging (>450) (Taylor et al., 1996), thus more points might provide more comparable results.

5. Conclusions

This study uses the full power of an analytical method that holds great promise for remote, in situ planetary surface mineralogy, laser Raman Spectroscopy, to investigate <45 μm grains in four endmember lunar soils. Major, minor, and trace minerals were identified. Among them the Raman peak positions of a few quartz grains indicate a limited range of impact pressures. The compositional characteristics of the major minerals extracted from the Raman spectra are consistent with those obtained by compositional analysis methods (although not nearly as precise as electron- and ion-beam methods or laser ablation ICP-MS). Furthermore, we were able to obtain additional information on the compositional distributions for solid-solution minerals (olivine and pyroxene). The mineral modes obtained for lunar soils (e.g., 14163, 71501) are consistent with studies based on use of optical petrography and electron-microprobe particle counting methods and X-ray imaging methods. More importantly, knowledge of the mineralogy resulting from the Raman point-counting procedures provide tests and validation for future in situ surface exploration using laser Raman spectroscopy. Through this study, we confirm that laser Raman spectroscopy can be a powerful tool in future lunar surface missions for the characterization of surface materials at scientifically interesting areas, as well as for in situ resource utilization.

Acknowledgments

This study was initiated by a collaboration between School of Space Sciences and Physics at Shandong University and Dept. Earth and Planetary Sciences at Washington University, and supported by both institutions. We thank Randy L. Korotev for his helpful reviews and comments on this manuscript. Zongcheng Ling appreciate the support from China Postdoctoral Science Foundation (Grant No. 20090450580), the National Natural Science Foundation of China (Grant No. 11003012), the National High Technology Research and Development Program of China (No. 2008AA12A212), and the Young Researcher Grant of the National Astronomical Observatories, Chinese Academy of Sciences, during the preparation of this manuscript. The authors thank two anonymous reviewers whose constructive comments are very helpful in improving the quality of the paper.

References

- Angel, R.J., 1988. High-pressure structure of anorthite. *Am. Mineral.* 73, 1114–1119.
- Basu, A., McKay, D.S., 1979. Petrography and provenance of Apollo 15 soils. *Proc. Lunar Sci. Conf.* 10, 1413–1424.
- Carr, M., Meyer, C., 1972. Chemical and petrographic characterization of Fra Mauro soils. *Proc. Lunar Sci. Conf.* 3, *Geochim. Cosmochim. Acta* 1 (Suppl. 3), 1015–1027.
- Chopelas, A., 1991. Single-crystal Raman-spectra of forsterite, fayalite, and monticellite. *Am. Mineral.* 76, 1101–1109.
- Chopelas, A., 1999. Estimates of mantle relevant Clapeyron slopes in the MgSiO₃ system from high-pressure spectroscopic data. *Am. Mineral.* 84, 233–244.
- Daniel, I., Gillet, P., Ghose, S., 1995. A new high-pressure phase-transition in anorthite (CaAl₂Si₂O₈) revealed by Raman-spectroscopy. *Am. Mineral.* 80, 645–648.
- Daniel, I., Gillet, P., McMillan, P.F., Wolf, G., Verhelst, M.A., 1997. High-pressure behavior of anorthite: Compression and amorphization. *J. Geophys. Res.* 102, 10313–10325.
- Dele-Dubois, M.L., Dhameincourt, P., Schubnel, H.J., 1980. Etude par spectroscopie Raman d'inclusions dans les diamants, saphirs et émeraudes/2. *Rev. Gemmol. AFG* 64, 11–14.
- Etchepare, J., Merian, M., Smetankine, L., 1974. Vibrational normal modes of SiO₂. I. α and β quartz. *J. Chem. Phys.* 60, 1873–1876.
- Fabel, G.W., White, W.B., White, E.W., Roy, R., 1972. Structure of lunar glasses by Raman and soft X-ray spectroscopy. *Proc. Lunar Sci. Conf.* 3, *Geochim. Cosmochim. Acta* 1 (Suppl. 3), 939–951.
- Finkelman, R., 1973. Analysis of the ultrafine fraction of the Apollo 14 regolith. *Proc. Lunar Sci. Conf.* 4, *Geochim. Cosmochim. Acta* 1 (Suppl. 4), 179–189.
- Fischer, E.M., Pieters, C.M., 1995. Lunar-surface aluminum and iron concentration from Galileo solid-state imaging data, and the mixing of mare and highland materials. *J. Geophys. Res.* 100, 23279–23290.
- Freeman, J.J., Wang, A., Kuebler, K.E., Jolliff, B.L., Haskin, L.A., 2008. Characterization of natural feldspars by Raman spectroscopy for future planetary exploration. *Can. Mineral.* 46, 1477–1500.
- Graf, J.C., 1993. Lunar soils Grain Size Catalog. NASA Ref. Pub. 1265.
- Haskin, L.A., Wang, A., Rockow, K.M., Jolliff, B.L., Korotev, R.L., Viskupic, K.M., 1997. Raman spectroscopy for mineral identification and quantification for in situ planetary surface analysis: A point count method. *J. Geophys. Res.* 102, 19293–19306.
- Heiken, G., McKay, D., 1974. Petrography of Apollo 17 soils. *Proc. Lunar Sci. Conf.* 5, *Geochim. Cosmochim. Acta* 1 (Suppl. 5), 843–860.
- Heiken, G., Vaniman, D.T., French, B.M., 1991. *Lunar Sourcebook: A User's Guide to the Moon*. Lunar and Planetary Institute and Cambridge University Press.
- Iishi, K., 1978. Lattice dynamics of forsterite. *Am. Miner.* 63, 1198–1208.
- Johnson, J.R., Hörz, F., Lucey, P.G., Christensen, P.R., 2002. Thermal infrared spectroscopy of experimentally shocked anorthosite and pyroxenite: Implications for remote sensing of Mars. *J. Geophys. Res.* 107. doi:10.1029/2001JE001517.

- Jolliff, B.L., 1991. Fragments of quartz monzodiorite and feldspar in Apollo-14 soil particles. *Proc. Lunar Sci. Conf.* 21, 101–118.
- Jolliff, B.L., Korotev, R.L., Haskin, L.A., 1991. Geochemistry of 2–4-Mm particles from Apollo-14 soil (14161) and implications regarding igneous components and soil-forming processes. *Proc. Lunar Sci. Conf.* 21, 193–219.
- Jolliff, B.L., Gillis, J.J., Haskin, L.A., Korotev, R.L., Wieczorek, M.A., 2000. Major lunar crustal terranes: Surface expressions and crust–mantle origins. *J. Geophys. Res.* 105, 4197–4216.
- Jolliff, B.L., Haskin, L.A., 1995. Cogenetic rock fragments from a lunar soil – Evidence of a ferroan noritic-anorthosite pluton on the Moon. *Geochim. Cosmochim. Acta* 59, 2345–2374.
- Jolliff, B.L., Hughes, J.M., Freeman, J.J., Zeigler, R.A., 2006. Crystal chemistry of lunar merrillite and comparison to other meteoritic and planetary suites of whitlockite and merrillite. *Am. Mineral.* 91, 1583–1595.
- Kempster, C.E., Megaw, H.D., Radoslovich, E.W., 1962. The structure of anorthite, $\text{CaAl}_2\text{Si}_2\text{O}_8$: 1. Structure analysis. *Acta Crystallogr.* 15, 1005–1017.
- Korotev, R.L., 1997. Some things we can infer about the Moon from the composition of the Apollo 16 regolith. *Meteorit. Planet. Sci.* 32, 447–478.
- Korotev, R.L., Jolliff, B.L., Zeigler, R.A., Gillis, J.J., Haskin, L.A., 2003. Feldspathic lunar meteorites and their implications for compositional remote sensing of the lunar surface and the composition of the lunar crust. *Geochim. Cosmochim. Acta* 67, 4895–4923.
- Korotev, R.L., Wang, A., Haskin, L.A., Jolliff, B.L., 1998. A Raman point-count study of Apollo 17 soil. *Lunar Planet. Sci. XXIX*, #1797.
- Kuebler, K.E., Jolliff, B.L., Wang, A., Haskin, L.A., 2006. Extracting olivine (Fo–Fa) compositions from Raman spectral peak positions. *Geochim. Cosmochim. Acta* 70, 6201–6222.
- Labotka, T.C., Kempa, M.J., White, C., Papike, J.J., Laul, J.C., 1980. The lunar regolith – Comparative petrology of the Apollo sites. *Proc. Lunar Planet. Sci. Conf.* 11, 1285–1305.
- Laul, J.C., Papike, J.J., 1980. The lunar regolith – Comparative chemistry of the Apollo sites. *Proc. Lunar Sci. Conf.* 11, 1307–1340.
- Lewis, J.S., Lewis, R.A., 1987. *Space Resources. Breaking the Bonds of Earth.* Columbia University Press, New York.
- Lewis, J.S., Matthews, M.S., Guerrieri, M.L. (Eds.), 1993. *Resources of near-Earth space.* The University of Arizona Press, Tucson & London.
- Linton, J.A., Fei, Y.W., Navrotsky, A., 1999. The MgTiO_3 – FeTiO_3 join at high pressure and temperature. *Am. Mineral.* 84, 1595–1603.
- Lucey, P., Korotev, R.L., Gillis, J.J., Taylor, L.A., Lawrence, D., Campbell, B.A., Elphic, R., Feldman, B., Hood, L.L., Huntten, D., 2006. Understanding the lunar surface and space–Moon interactions. *Rev. Mineral. Geochem.* 60, 83–219 (Chapter 2).
- Matson, D.W., Sharma, S.K., Philpotts, J.A., 1986. Raman spectra of some tectosilicates and of glasses along the orthoclase–anorthite and nepheline–anorthite joins. *Am. Mineral.* 71, 694–704.
- McCord, T., Adams, J., 1973. Progress in remote optical analysis of lunar surface composition. *The Moon* 7, 453–474.
- McCord, T., Johnson, T., 1970. Lunar spectral reflectivity (0.30 to 2.50 microns) and implications for remote mineralogical analysis. *Science* 169, 855–858.
- McMillan, P.F., 1984. Structural studies of silicate glasses and melts – Applications and limitations of Raman spectroscopy. *Am. Mineral.* 69, 622–644.
- McMillan, P.F., Ross, N.L., 1987. Heat capacity calculations for Al_2O_3 corundum and MgSiO_3 ilmenite. *Phys. Chem. Mineral.* 14, 225–234.
- McMillan, P.F., Wolf, G.H., Lambert, P., 1992. A Raman-spectroscopic study of shocked single crystalline quartz. *Phys. Chem. Mineral.* 19, 71–79.
- Megaw, R., Kempster, C.J.E., Radoslovich, E.W., 1962. The structure of anorthite, $\text{CaAl}_2\text{Si}_2\text{O}_8$: II. Description and discussion. *Acta Crystallogr.* 15, 1017–1035.
- Mendell, W.W., 1985. *Lunar Bases and Space Activities of the 21st Century.* Lunar and Planetary Institute, Houston.
- Mernagh, T.P., 1991. Use of the laser Raman microprobe for discrimination amongst feldspar minerals. *J. Raman Spectrosc.* 22, 453–457.
- Morris, R.V., 1978. The surface exposure /maturity/ of lunar soils – Some concepts and *Is/FeO* compilation. *Proc. Lunar Sci. Conf.* 9, 2287–2297.
- Morris, R.V., Score, R., Dardano, C., Heiken, G., 1983. *Handbook of Lunar Soils, JSC 19069.* NASA Johnson Space Center, Houston, 914 pp.
- Muehlberger, W., Horz, F., Sevier, J., Ulrich, G., 1980. Mission objectives for geological exploration of the Apollo 16 landing site. *Proc. Conf. Lunar Highlands Crust.* 1–49.
- Noble, S.K., Pieters, C.M., Taylor, L.A., Morris, R.V., Allen, C.C., McKay, D.S., Keller, L.P., 2001. The optical properties of the finest fraction of lunar soil: Implications for space weathering. *Meteorit. Planet. Sci.* 36, 31–42.
- Ohashi, H., Sekita, M., 1982. Raman spectroscopic study of the Si–O–Si stretching vibration in clinopyroxenes. *J. Jpn. Assoc. Mineral., Petrol. Econ. Geol.* 77, 455–459.
- Papike, J.J., 1987. Chemistry of the rock-forming silicates: Ortho, ring, and single-chain structures. *Rev. Geophys.* 25, 1483–1526.
- Papike, J.J., 1988. Chemistry of the rock-forming silicates: Multiple-chain sheet, and framework structures. *Rev. Geophys.* 26, 407–444.
- Papike, J.J., Ryder, G., Shearer, C.K., 1998. Lunar samples. *Mineral. Soc. Am. Rev. Mineral.* 36, 5–1–5–234.
- Paques-Ledent, M.T., Tarte, P., 1973. Vibrational studies of olivine-type compounds—I. The IR and Raman spectra of the isotopic species of Mg_2SiO_4 . *Spectrochim. Acta A* 29, 1007–1016.
- Perry, C.H., Agrawal, D.K., Anastassakis, E., Lowndes, R.P., Rastogi, A., Tornberg, N.E., 1972. Infrared and Raman spectra of lunar samples from Apollo 11, 12 and 14. *Earth Moon Planets* 4, 315–336.
- Pieters, C., Shkuratov, Y., Kaydash, V., Stankevich, D., Taylor, L., 2006. Lunar soil characterization consortium analyses: Pyroxene and maturity estimates derived from Clementine image data. *Icarus* 184, 83–101.
- Pieters, C.M., Fischer, E.M., Rode, O., Basu, A., 1993. Optical effects of space weathering – The role of the finest fraction. *J. Geophys. Res.* 98, 20817–20824.
- Pieters, C.M., Taylor, L.A., Noble, S.K., Keller, L.P., Hapke, B., Morris, R.V., Allen, C.C., McKay, D.S., Wentworth, S., 2000. Space weathering on airless bodies: Resolving a mystery with lunar samples. *Meteorit. Planet. Sci.* 35, 1101–1107.
- Price, G.D., Parker, S.C., Leslie, M., 1987. The lattice dynamics of forsterite. *Mineral. Mag.* 51, 157–170.
- Quick, J., Albee, A., James, O., 1981. Petrology and petrogenesis of lunar breccia 12013. *Proc. Lunar Sci. Conf.* 12B, 117–172.
- Ross, N.L., McMillan, P.F., 1984. The Raman spectrum of MgSiO_3 ilmenite. *Am. Mineral.* 69, 719–721.
- Sharma, S.K., Lucey, P.G., Ghosh, M., Hubble, H.W., Horton, K.A., 2003. Stand-off Raman spectroscopic detection of minerals on planetary surfaces. *Spectrochim. Acta A* 59, 2391–2407.
- Sharma, S.K., Simons, B., Yoder, H.S., 1983. Raman study of anorthite, calcium Tschermak's pyroxene, and gehlenite in crystalline and glassy states. *Am. Mineral.* 68, 1113–1125.
- Simon, S., Papike, J., Laul, J., 1981. The lunar regolith – Comparative studies of the Apollo and Luna sites. *Petrology of soils from Apollo 17, Luna 16, 20, and 24.* *Proc. Lunar Sci. Conf.* 12B, 371–388.
- Spudis, P.D., 1984. Apollo-16 site geology and impact melts – Implications for the geologic history of the lunar highlands. *J. Geophys. Res.* 89, C95–C107.
- Taylor, L.A., Patchen, A., Taylor, D.H.S., Chambers, J.G., McKay, D.S., 1996. X-ray digital imaging petrography of lunar mare soils: Modal analyses of minerals and glasses. *Icarus* 124, 500–512.
- Taylor, L.A., Pieters, C., Keller, L.P., Morris, R.V., McKay, D.S., Patchen, A., Wentworth, S., 2001. The effects of space weathering on Apollo 17 mare soils: Petrographic and chemical characterization. *Meteorit. Planet. Sci.* 36, 285–299.
- Taylor, S., Kaye, M., Muir, P., Nance, W., Rudowski, R., Ware, N., 1972. Composition of the lunar uplands: Chemistry of Apollo 14 samples from Fra Mauro. *Proc. Lunar Sci. Conf.* 3, *Geochim. Cosmochim. Acta* 2 (Suppl. 3), 1231–1249.
- Wang, A., Haskin, L.A., Lane, A.L., Wdowiak, T.J., Squyres, S.W., Wilson, R.J., Hovland, L.E., Manatt, K.S., Raouf, N., Smith, C.D., 2003. Development of the Mars microbeam Raman spectrometer (MMRS). *J. Geophys. Res.* 108, 5005. doi:10.1029/2002JE001902, 2003.
- Wang, A., Jolliff, B.L., Haskin, L.A., 1995. Raman-spectroscopy as a method for mineral identification on lunar robotic exploration missions. *J. Geophys. Res.* 100, 21189–21199.
- Wang, A., Jolliff, B.L., Haskin, L.A., Kuebler, K.E., Viskupic, K.M., 2001. Characterization and comparison of structural and compositional features of planetary quadrilateral pyroxenes by Raman spectroscopy. *Am. Mineral.* 86, 790–806.
- Wang, A., Kuebler, K., Jolliff, B., Haskin, L.A., 2004a. Mineralogy of a martian meteorite as determined by Raman spectroscopy. *J. Raman Spectrosc.* 35, 504–514.
- Wang, A., Kuebler, K.E., Jolliff, B.L., Haskin, L.A., 2004b. Raman spectroscopy of Fe–Ti–Cr-oxides, case study: Martian meteorite EETA79001. *Am. Mineral.* 89, 665–680.
- Warren, P.H., Taylor, G.J., Keil, K., Shirley, D.N., Wasson, J.T., 1983. Petrology and chemistry of 2 large granite clasts from the Moon. *Earth Planet. Sci. Lett.* 64, 175–185.
- Wdowiak, T., Agresti, D., Mirov, S., 1995. A laser Raman system suitable for incorporation into lander spacecraft. *Lunar Planet. Sci. XXVI*, 1473–1474.
- White, W.B., 1975. *Structural Interpretation of Lunar and Terrestrial Minerals by Raman Spectroscopy Infrared and Raman Spectroscopy of Lunar and Terrestrial Minerals by Raman Spectroscopy.* Academic Press, Inc., New York. pp. 325–358.